Journal of Controlled Release xxx (xxxx) xxx

Contents lists available at ScienceDirect

Journal of Controlled Release

journal homepage: www.elsevier.com/locate/jconrel

Brain delivery of Plk1 inhibitor *via* chimaeric polypeptide polymersomes for safe and superb treatment of orthotopic glioblastoma

Qianyi Fan, Yuanyuan Liu, Guanhong Cui, Zhiyuan Zhong *, Chao Deng *

Biomedical Polymers Laboratory, Jiangsu Key Laboratory of Advanced Functional Polymer Design and Application, College of Chemistry, Chemical Engineering and Materials Science, State Key Laboratory of Radiation Medicine and Protection, Soochow University, Suzhou 215123, China

ARTICLE INFO

Keywords:
Polypeptide
Polymersome
Glioblastoma
Blood-brain barrier
Targeted delivery

ABSTRACT

The chemotherapy toward glioblastoma (GBM) is severely challenged by blood-brain barrier and dose-limiting toxicity. Herein, we adopt brain delivery of Plk1 inhibitor volasertib (Vol), which is highly specific and presents low off-target toxicity, as a new means to treat GBM, for which angiopep-2-docked chimaeric polypeptide polymersome (ANG-CPP) was designed and prepared from poly(ethylene glycol)-*b*-poly(L-tyrosine)-*b*-poly(L-aspartic acid) for loading Vol to its watery interior *via* electrostatic interactions. ANG-CPP loaded with 13.9 wt% Vol (ANG-CPP-Vol) exhibited a small size of about 76 nm, superb colloidal stability (against dilution, serum and long-term storage), and enzyme-triggered drug release behavior (about 73% of Vol released within 8 h with proteinase K). In sharp contrast to free Vol, ANG-CPP-Vol induced complete G2/M cell cycle arrest in U-87 MG GBM cells giving 7.8-times better anti-tumor activity, prolonged circulation time and largely increased GBM enrichment. ANG-CPP-Vol effectively suppressed the growth of orthotopic U-87 MG GBM and significantly boosted mice survival rate. Importantly, ANG-CPP-Vol showed further reduced toxicity over free Vol. This great safety and remarkable efficacy of ANG-CPP-Vol renders it a high potential for treating GBM.

1. Introduction

Glioblastoma (GBM) is the most destructive and malignant tumor in the brain with a five-year survival rate of only 5% [1–3]. Owing to the invasive growth of GBM, it is exceptionally difficult to acquire a decent therapeutic effect through either surgical or radiation treatment [4,5]. Meanwhile, the complexity and retardation of blood-brain barrier (BBB) greatly impede the delivery of chemical drugs to GBM, affording ineffective tumor drug concentration and poor pharmacological effects [6,7]. Recently, ligands facilitating BBB penetration like transferrin [8–10], cRGD peptide [11–15], glucose [16,17], and apolipoprotein E [18–20] have been utilized to boost the therapeutic effects of nano-drugs toward brain-associated diseases. Angiopep-2 (ANG), a specific ligand of lipoprotein receptor-related protein 1 (LRP-1) receptor, has shown an elevated BBB transport efficiency [21–24], and recently been decorated on nanotherapeutics containing different cytotoxic drugs such as doxorubicin, paclitaxel, docetaxel, arsenic trioxide to enhance BBB penetration and GBM treatment [25–29]. It should be noted, however, that in spite of improved GBM accumulation, cytotoxic drugs are inevitably accompanied with strong side effects.

The past years has seen a fast progress of molecular targeted drugs that are featured with high specificity, lessened off-target toxicity, and remarkable anti-cancer efficacy [30,31]. Of note, temozolomide targeted to DNA at O^6 position of guanine has shown to be capable of crossing BBB and inducing DNA damage and cell death of GBM [32,33]. Though temozolomide has become a gold standard treatment for GBM, the therapeutic benefits are limited by the short half-life and acquired drug resistance [34]. Polo-like kinase 1 (Plk1) was found highly expressed in GBM, and the inhibition of Plk1 led to effective growth suppression of GBM cells [35]. Among all the Plk1 inhibitors, volasertib (Vol) is the most successful and has been approved for treating patients with acute myeloid leukemia (AML) [36]. Vol has shown to specifically inhibit Plk1 through binding to the terminal NH_2 and COOH groups of ATP binding pocket of Plk1 *via* hydrogen bonds, thus can prevent activation of cyclin B-Cdk1 complex and arrest tumor cells at G2/M phase [37,38], leading to down-regulation of oncogenes and up-regulation of tumor suppressor genes [39,40]. We envisioned that brain delivery of Vol might be a novel treatment for GBM. Of note, there are few reports on delivery of Vol [41], let alone to GBM.

In this contribution, angiopep-2-docked chimaeric polypeptide polymersome (ANG-CPP) was adopted to achieve brain delivery of Vol to orthotopic human GBM model in mice (Scheme 1). ANG-CPP was

* Corresponding authors.
E-mail addresses: zyzhong@suda.edu.cn (Z. Zhong), cdeng@suda.edu.cn (C. Deng).

https://doi.org/10.1016/j.jconrel.2020.10.043
Received 25 July 2020; Received in revised form 6 October 2020; Accepted 21 October 2020
Available online 24 October 2020

designed with short poly(L-aspartic acid) in the interior for robust encapsulation of Vol and ANG on the surface for targeting to GBM. We have shown previously that micelles based on poly(ethylene glycol)-*b*-poly(L-tyrosine) (PEG-*b*-PTyr) are robust as a result of π-π stacking while quickly release payloads inside cancer cells due to enzymatic degradation [42,43]. This represents the first report on targeted molecular therapy of GBM with Vol. Our results revealed that ANG-CPP markedly increased GBM enrichment and further reduced the off-target toxicity of Vol, leading to effective inhibition of orthotopically xenografted U-87 GBM and significant survival advantages.

2. Experimental methods

2.1. Synthesis of mPEG-b-PTyr-b-PAsp and ANG-PEG-b-PTyr

Firstly, mPEG-NH_2 (M_n = 5.0 kg/mol) was used as a macroinitiator to sequentially initiate the polymerization of L-tyrosine *N*-carboxyanhydride (Tyr-NCA) and β-benzyl-L-aspartate *N*-carboxyanhydride (BLA-NCA) monomers. Under a nitrogen atmosphere, to a solution of mPEG-NH_2 (0.38 g, 0.080 mmol) in DMF (3.8 mL) was rapidly added Tyr-NCA (1.20 g, 5.60 mmol) solution in DMF (12.0 mL). After stirring at 37 °C under N_2 for 72 h, BLA-NCA (0.33 g, 1.30 mmol) solution in DMF was added and the reaction proceeded at 37 °C for another 72 h. Following the precipitation in an excess of diethyl ether, the mPEG-*b*-PTyr-*b*-PBLA product was further purified by redissolving in dichloromethane and precipitating in diethyl ether thrice. Yield: 88%. ^{1}H NMR (400 MHz, DMSO-d_6, Fig. S1, δ): 9.10 (-C_6H_4OH), 7.95 (-CHN*H*CO-), 7.31 (-C_6H_5), 6.94 and 6.59 (-C_6H_4OH), 5.04 ($C_6H_5CH_2$-), 4.42 (-COC*H*NH-), 3.50 (-OCH_2CH_2O-), 3.43(-OCH_3), 2.82–2.63 (-$C_6H_4CH_2$-, -COCH_2CH-). PEG-*b*-PTyr-*b*-PAsp was acquired by deprotection of PEG-*b*-PTyr-*b*-PBLA using HBr. Typically, HBr (5.03 mmol, 33 wt% in HOAc, 0.9 mL) was added to a solution of PEG-*b*-PTyr-*b*-PBLA (0.87 g, 0.047 mmol) in trifluoroacetic acid (8.7 mL) at 0 °C. After stirring for 2 h, the mixture was precipitated with diethyl ether to obtain PEG-*b*-PTyr-*b*-PAsp. Yield: 83%. ^{1}H NMR (400 MHz, DMSO-d_6, Fig. 1A, δ): 7.95 (-CHN*H*CO-), 6.95 and 6.59 (-C_6H_4OH), 4.41 (-COC*H*NH-), 3.50 (-OCH_2CH_2O-), 3.24 (-OCH_3), 2.82–2.63 (-$C_6H_4CH_2$-, -COCH_2CH-).

ANG-PEG-*b*-PTyr was obtained through the thiol-ene click reaction between thiol group of ANG and maleimide-terminated PEG-*b*-PTyr (MAL-PEG-*b*-PTyr) that was similarly synthesized *via* controlled polymerization of Tyr-NCA using MAL-PEG-NH_2 as an initiator. Yield: 83%. ^{1}H NMR (400 MHz, DMSO-d_6, Fig. S2, δ): 9.10 (-O*H*), 7.95 (-CHN*H*CO-), 6.95 and 6.59 (-C_6H_4OH), 6.77 (MAL), 4.42 (-COC*H*NH-), 3.50 (-OCH_2CH_2O-), 2.83–2.63 (-$C_6H_4CH_2$). ANG (20 mg, 8.8 nmol) was conjugated onto MAL-PEG-*b*-PTyr (100 mg, 5.9 nmol) through thiol-ene click reaction in DMSO for 24 h. The raw product was purified through sequential dialysis (MWCO 7000 Da) against DMSO for 24 h and deionized water for 48 h followed by lyophilization to obtain ANG-PEG-

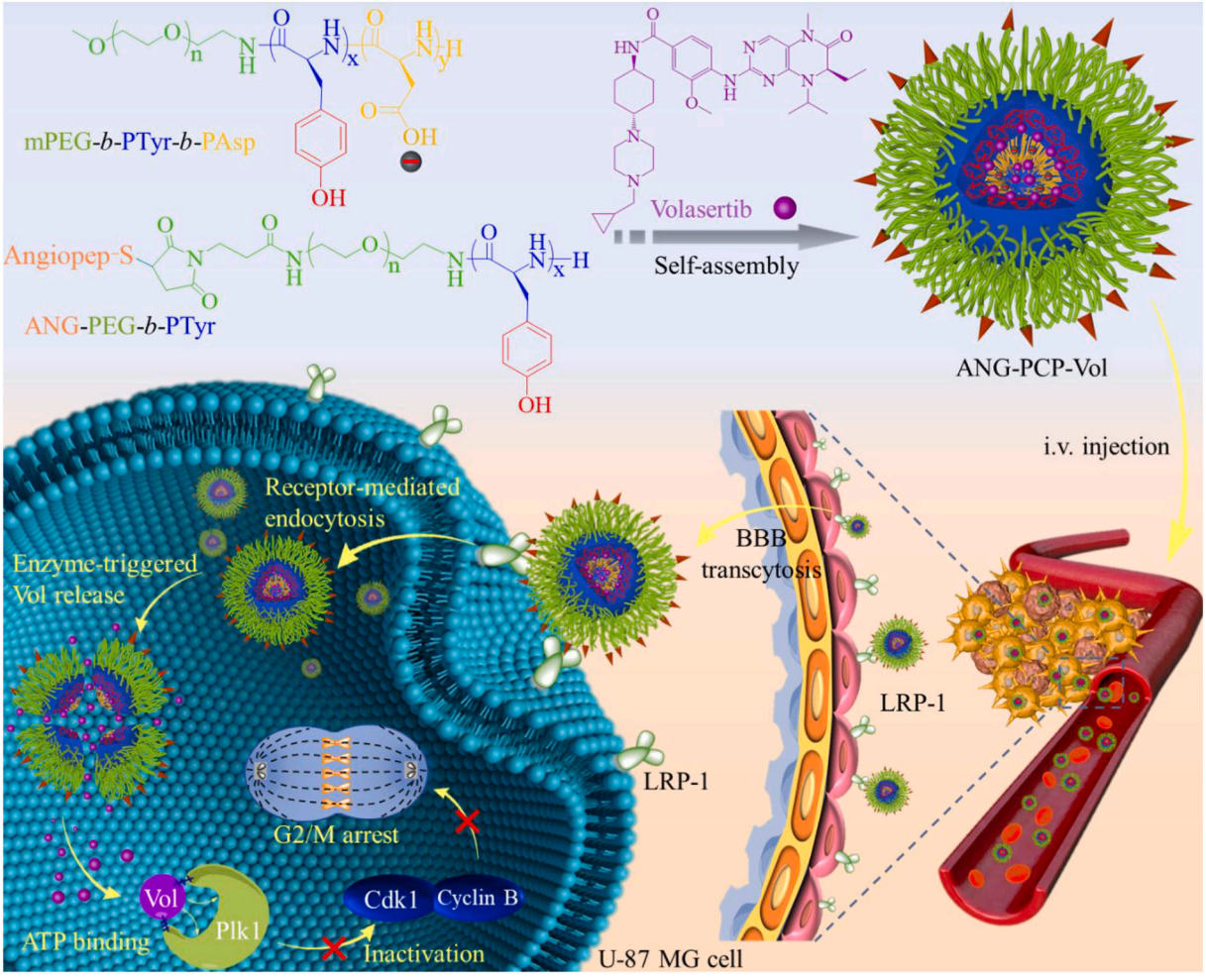

Scheme 1. Volasertib (Vol)-loaded angiopep-2-decorated chimaeric polypeptide polymersome (ANG-CPP-Vol) for safe and superb therapy of human glioblastoma (GBM) model. ANG-CPP-Vol self-assembled from PEG-*b*-PTyr-*b*-PAsp can effectively cross BBB and GBM membrane through LRP-1-mediated transcytosis and endocytosis, respectively. The enzyme-triggered Vol release from ANG-CPP-Vol significantly inhibits the expression of Plk1 protein and further induces G2/M cell cycle arrest in U-87 cancer cells.

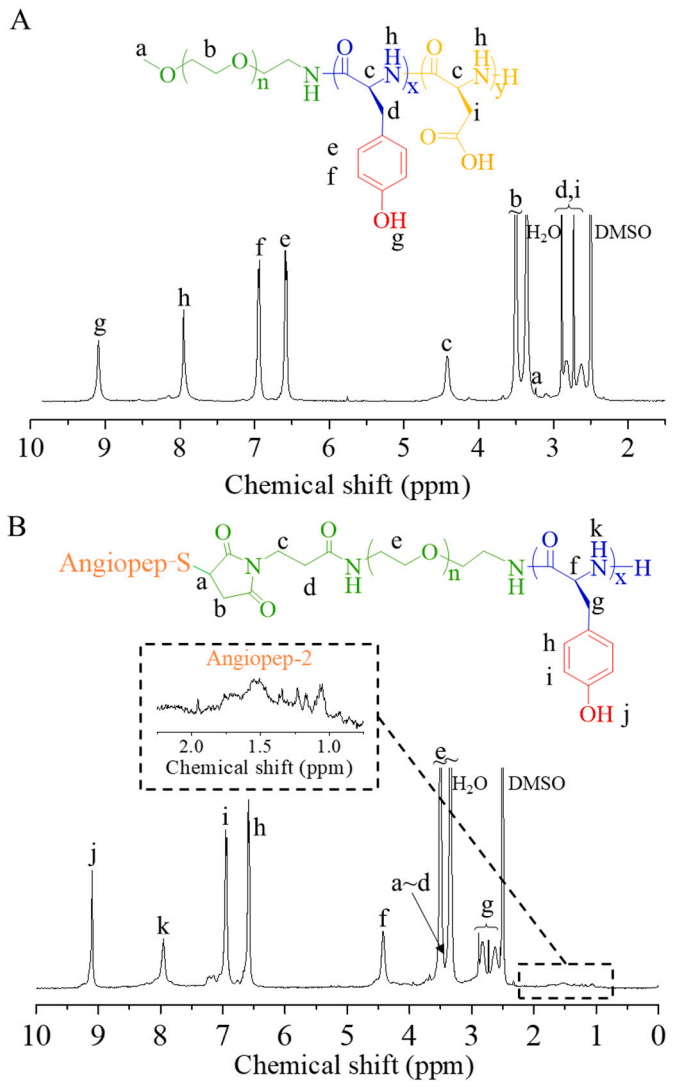

Fig. 1. ^{1}H NMR spectra (400 MHz, DMSO-d_6) of mPEG-*b*-PTyr-*b*-PAsp (A) and ANG-PEG-*b*-PTyr (B).

b-PTyr. Yield: 91%. ^{1}H NMR (400 MHz, DMSO-d_6, Fig. 1B, δ): 9.10 (-C_6H_4OH), 7.95 (-CHN*H*CO-), 6.93 and 6.59 (-C_6H_4OH-), 4.40 (-COC*H*NH-), 3.50 (-OCH_2CH_2O-), 2.84–2.63 (-$C_6H_4CH_2$), 0.93–1.95 (ANG). The degree of ANG conjugation was quantified by bicinchoninic acid (BCA) protein assay.

2.2. Preparation of ANG-CPP-Vol

Vol was readily loaded into ANG-CPP *via* a solvent-exchange method. Briefly, the mixed solution (10.0 mg/mL, 100 μL) consisting of ANG-PEG-*b*-PTyr, mPEG-*b*-PTyr-*b*-PAsp, and Vol (10.0 mg/mL, 12.5 μL) was dropwise added to PB buffer (pH 8.0, 5.0 mM, 900 μL) under stirring at room temperature. Thus formed ANG-CPP-Vol was extensively dialyzed against PB for 8 h (MWCO 3500 Da) to remove free Vol. The dialysis medium was replaced every hour. The colloidal stability of ANG-CPP-Vol against dilution, 10% fetal bovine serum (FBS) and long-term storage was investigated by monitoring its size change using dynamic light scattering (DLS). The enzymatic responsivity of ANG-CPP-Vol was evaluated following the incubation with proteinase K (6.0 Units/mL) in Tris-HCl (10 mM, pH 7.4) at 37 °C under shaking (200 rpm). The Vol amount was quantified by UV–Vis spectroscopy at 330 nm, and the drug-loading content (DLC) as well as drug-loading efficiency (DLE) of ANG-CPP-Vol were determined according to the following formulas:

$$\text{DLC (wt\%)} = (\text{weight of loaded Vol}/\text{weight of ANG} - \text{CPP} - \text{Vol}) \times 100$$

$$\text{DLE (\%)} = (\text{weight of loaded Vol}/\text{weight of fed Vol}) \times 100$$

2.3. Cytotoxicity and cell cycle arrest of ANG-CPP-Vol

The toxicity of ANG-CPP-Vol to U-87 MG cells was evaluated by the 3-(4,5-dimethylthiazol-2-yl)-2,5-diphenyltetrazolium bromide (MTT) assay. The cells were cultured in a 96-well plate at a density of 3×10^3 cells/well for 24 h with DMEM medium, followed by adding free Vol, CPP-Vol and ANG-CPP-Vol at varying concentrations. After incubating for 4 h, the culture medium was refreshed and the cells were incubated for an additional 68 h. Then, the above medium was treated with 0.5 mg/mL of MTT (10 μL) for 4 h and replaced with 150 μL of dimethyl sulfoxide to dissolve the purple formazan crystals produced by the living cells. The absorbance of formazan at 570 nm was acquired by a microplate reader, and the percentages of viable cells were compared with PBS group to determine the cell viability. The cytotoxicity of blank ANG-CPP to U-87 MG cells and ANG-CPP-Vol to L929 cells were similarly evaluated by MTT assays following 48 h incubation with cells.

For cell cycle arrest evaluation, U-87 MG cells were seeded at a density of 2×10^5 cells/well for 24 h in a 6-well plate. The cells following the treatment with free Vol, CPP-Vol and ANG-CPP-Vol (Vol concentration: 0.5 μg/mL) for 4 h were further cultured with fresh medium for 20 h. The cells were trypsinized, washed three times with PBS, and precipitated by centrifugation (1000 rpm × 3 min). The collected cells following the dispersion in 1.0 mL PBS were slowly added to 4.0 mL of ethanol (95%, v/v) under ice bath, and stored in a refrigerator at 4 °C for 24 h. After centrifugation, the propidium iodide (PI) staining solution containing RNase A was added to the cells in the dark, and stained for 30 min. The number of cells at different stages of the cell cycle was analyzed using flow cytometry (488 nm).

2.4. GBM targeted accumulation

The mice were handled under protocols approved by Soochow University Laboratory Animal Center and the Animal Care and Use Committee of Soochow University. The distribution of CPP-Vol and ANG-CPP-Vol *in vivo* was studied using orthotopic U-87 MG-Luc tumor xenografts that were established by implanting minced tumor tissue into the left striatum of female BALB/c nude mice [20]. After intravenous injection of Cy5-labeled CPP-Vol or ANG-CPP-Vol (40 μg Cy5 equiv./animal) into the mice, the fluorescence imaging of mice was obtained at 0, 4, 8, 12, 24, 48 h using an *in vivo* near-infrared fluorescence imaging system ($\lambda_{Ex} = 747$ nm, $\lambda_{Em} = 774$ nm). For *ex vivo* imaging, GBM-bearing mice was sacrificed to obtain brain tissue at 12, 24, or 48 h post-injection of Cy5-ANG-CPP-Vol/FITC, Cy5-CPP-Vol/FITC and free Vol/FITC (40 μg Cy5 equiv./animal, 50 μg FITC equiv./animal). The brain containing GBM was fixed in 4% paraformaldehyde for 24 h and then cut into 5 μm thick tissue in paraffin by Servicebio Company. After staining the nucleus with 4′,6-diamidino-2-phenylindole (DAPI, 1.0 μg/mL) for 10 min, the distribution of Cy5-ANG-CPP-Vol/FITC, Cy5-CPP-Vol/FITC and free Vol/FITC in the tumor area was observed by confocal microscopy (LSM710, Leica, Germany).

2.5. In vivo antitumor efficacy

The *in vivo* antitumor efficacy was evaluated in orthotopic U-87 MG-Luc GBM xenografts. The day of implanting tumor tissue was defined as day 0. On day 5, orthotopic U-87 MG-Luc GBM-bearing mice were intraperitoneal injected with 75 mg/kg D-Luciferin potassium salt as the substrate for firefly luciferase, to monitor tumor bioluminescence. The mice were divided into 4 groups ($n = 7$), administered with free Vol, CPP-Vol, or ANG-CPP-Vol (Vol, 10 mg/kg) *via* the tail vein every 2 days

for 6 times. The tumor growth of mice treated with different formulations were monitored using bioluminescence imaging on day 5, 8, and 12. Meanwhile, the change of body weight and survival time of the mice during the whole treatment were recorded. On day 14, a representative mouse from each group was sacrificed, and their main organs and tumor-bearing brain tissue were excised and fixed in a 4% formalin solution for histological analysis.

2.6. Statistical analysis

All data were presented as mean ± standard deviation (SD). Statistical differences between groups were assessed by one-way analysis of variance (ANOVA). Kaplan–Meier survival curves were constructed by log-rank test for comparisons. Statistical significance was defined as $^{*}p < 0.05$, $^{**}p < 0.01$, $^{***}p < 0.001$.

3. Results and discussion

3.1. Synthesis of mPEG-b-PTyr-b-PAsp and ANG-PEG-b-PTyr

mPEG-*b*-PTyr-*b*-PAsp copolymer was synthesized by sequential copolymerization of Tyr-NCA and BLA-NCA monomers using mPEG-NH_2 as an initiator, followed by removal of the benzyl protecting group (Scheme S1). ^{1}H NMR spectrum of mPEG-*b*-PTyr-*b*-PBLA discerned characteristic signals of mPEG (δ 3.50), PTyr (δ 9.10, 6.94, 6.59) and PBLA (δ 7.31, 5.04) (Fig. S1). The *DP* of PTyr and PBLA blocks calculated by comparing the integrals of signal at δ 3.50 (methylene of PEG) with those at δ 6.94, 6.59 (phenol of PTyr) and δ 7.31 (benzyl of PBLA) was 58 and 18, respectively (Table 1). The complete removal of protecting group was corroborated by the disappearance of signal at δ 7.31 owing to benzyl protection group (Fig. 1A). GPC measurement revealed that mPEG-*b*-PTyr-*b*-PAsp had a narrow distribution with an M_w/M_n of 1.11.

MAL-PEG-*b*-PTyr copolymer was similarly synthesized through NCA polymerization by using MAL-PEG-NH_2 as a macroinitiator. ^{1}H NMR spectrum of MAL-PEG-*b*-PTyr discerned characteristic signals of MAL-PEG (δ 6.77, 3.50) and PTyr (δ 9.10, 6.95, 6.59) (Fig. S2). The *DP* of the PTyr blocks measured by comparing the integrals of the signals at δ 6.95 and δ 3.50 was 71. The thiol-ene click reaction between MAL-PEG-*b*-PTyr and thiol group of ANG peptide was carried out in DMSO at 37 °C (Scheme S2). ^{1}H NMR spectrum of ANG-PEG-*b*-PTyr showed that the peak of ANG appeared at δ 0.93–1.95, indicating the successful conjugation of ANG (Fig. 1B). The degree of ANG conjugation of ANG-PEG-*b*-PTyr was further quantified to be 90% by BCA assay.

3.2. Preparation of ANG-CPP-Vol, drug loading, and enzyme-triggered drug release

ANG-CPP assembled from mPEG-*b*-PTyr-*b*-PAsp and ANG-PEG-*b*-PTyr displayed mean sizes of around 70 nm with narrow size distributions (Fig. S3) and slightly negative surface charge of around −12 mV (Table S1). With increasing ANG density from 10 mol% to 30 mol%, ANG-CPP exhibited slightly enlarged sizes from 69 to 79 nm (Table S1). Taking ANG-CPP with 20 mol% of ANG density as a typical example, we have evaluated the physicochemical properties of ANG-CPP. TEM images visualized that ANG-CPP had spherical morphology and homogeneous size distribution (Fig. 2A). Atomic force microscopy (AFM) image exhibited that ANG-CPP had well-defined shape and donut structure (Fig. 2B), in which the diameters were much bigger than the heights (Fig. 2C), signifying the vesicle structure of ANG-CPP. The R_g/R_h ratio (R_g: radius of gyration; R_h: radius of hydrodynamics) of ANG-CPP measured by multi-angle laser light scattering was about 1.03, further corroborating that ANG-CPP had a polymersomal structure. Circular dichroism (CD) measurement revealed that ANG-CPP had dominant β-sheet structure (Fig. S4).

Table 1
Synthesis of mPEG-*b*-PTyr-*b*-PAsp and MAL-PEG-*b*-PTyr copolymers.

Copolymers	M_n (kg/mol)		M_w/M_n [b]	Yield (%)
	Design	^{1}H NMR [a]		
mPEG-*b*-PTyr-*b*-PAsp	5-10-2	5-9.5-1.8	1.11	86
MAL-PEG-*b*-PTyr	5–12	5–11.5	1.09	89

[a] Calculated from ^{1}H NMR.
[b] Determined by GPC (eluent: DMF; flow rate: 0.8 mL/min; 40 °C; standard: poly(methyl methacrylate)).

Vol with a small molecular weight and amphiphilic nature can hardly be encapsulated in developed nanovehicles. Notably, robust loading of Vol with decent efficiencies of about 70% at theoretical drug loading contents of 5–20 wt% was accomplished with CPP and ANG-CPP (Table 2), mainly attributing to the electrostatic interactions between PAsp and Vol. The size of ANG-CPP-Vol increased from 63, 71 to 76 nm with increasing Vol contents from 5, 10, 20 wt%. ANG-CPP-Vol with 3.5 wt% and 7.3 wt% of Vol was about 10 and 2 nm smaller than blank ANG-CPP, in line with loading of Vol *via* electrostatic interactions. ANG-CPP-Vol exhibited negative surface charge changes which decreased from −13.5 to −7.9 mV with increasing Vol contents from 3.5 wt% to 13.9 wt %. Fig. 2D and Fig. S5 show that ANG-CPP-Vol was stable over dilution, 10% FBS, and one-week incubation in PBS (100 mM, pH 7.4). The high stability of ANG-CPP-Vol could be attributed to the presence of strong π-π stacking between phenolic groups of PTyr in the polymersomal membrane. The π-π stacking has been applied to formulate robust polymersomes and micelles [44–46]. In sharp contrast to chemical crosslinking that often involves tedious functionalization, coupling agents, and toxic catalyst, physical crosslinking *via* π-π stacking is simple, clean, and efficient. Proteinase K, a serine protease with wide cleavage activity, can efficiently cleave peptide bonds of aliphatic and aromatic amino acids, and has been widely utilized to evaluate the degradation behaviors of polypeptides and proteins [47,48]. In the presence of proteinase K, ANG-CPP-Vol swelled quickly in time with a mean size to 530 nm at 5.5 h (Fig. 2E) as a result from partial disruption of peptide bonds in both PTry and PAsp blocks. In accordance, release of Vol from ANG-CPP-Vol was markedly accelerated by proteinase K, in which about 73% and 23% of Vol was released within 12 h under proteinase K and physiological conditions, respectively (Fig. 2F).

3.3. Cellular uptake and BBB transcytosis of ANG-CPP-Vol

U-87 MG cells are known to overexpress LRP-1 receptors [49]. We and others have shown that ANG has a strong binding to U-87 MG cells [50–54]. The influence of ANG densities on cellular uptake by U-87 MG cells was firstly investigated by flow cytometry, and the results showed that ANG docking obviously enhanced the cellular uptake of CPP-Vol (Fig. 3A). ANG-CPP-Vol with 20 mol% of ANG displayed 2.3-fold better uptake than non-targeted CPP-Vol, and was selected for the following evaluation. Interestingly, ANG-CPP-Vol showed also better cellular uptake than free drug (Fig. S6). Meanwhile, U-87 MG cells treated with ANG-CPP-Vol for 4 h displayed strong Cy5 fluorescence derived from CPP and FITC fluorescence from Vol in cytosol as visualized by confocal microscopy (Fig. 3B & S7), indicating that efficient delivery and fast release of Vol were achieved by ANG-CPP. In contrast, much weaker FITC and Cy5 fluorescence was visualized in cells treated with CPP-Vol.

We further evaluated the BBB transcytosis of ANG-CPP-Vol using an *in vitro* model formed from bEnd.3 monolayer cells [20,55]. Fig. 3C shows that the value of trans-endothelial electrical resistance (TEER) of bEnd.3 monolayer was consistently above 200 $\Omega \cdot cm^2$ following 15 h incubation, suggesting it possesses decent integrity. The penetration studies demonstrated that ANG-CPP-Vol mediated obviously better BBB transcytosis than free Vol and CPP-Vol (Fig. 3D), mainly attributing to the specific binding of ANG to LRP-1 receptor that overexpressed on bEnd.3 cells of BBB [21,56]. 24-well plates having bEnd.3 monolayer in the upper chamber and U-87 MG cells in the lower chamber were employed to exploit both BBB transport and endocytosis function.

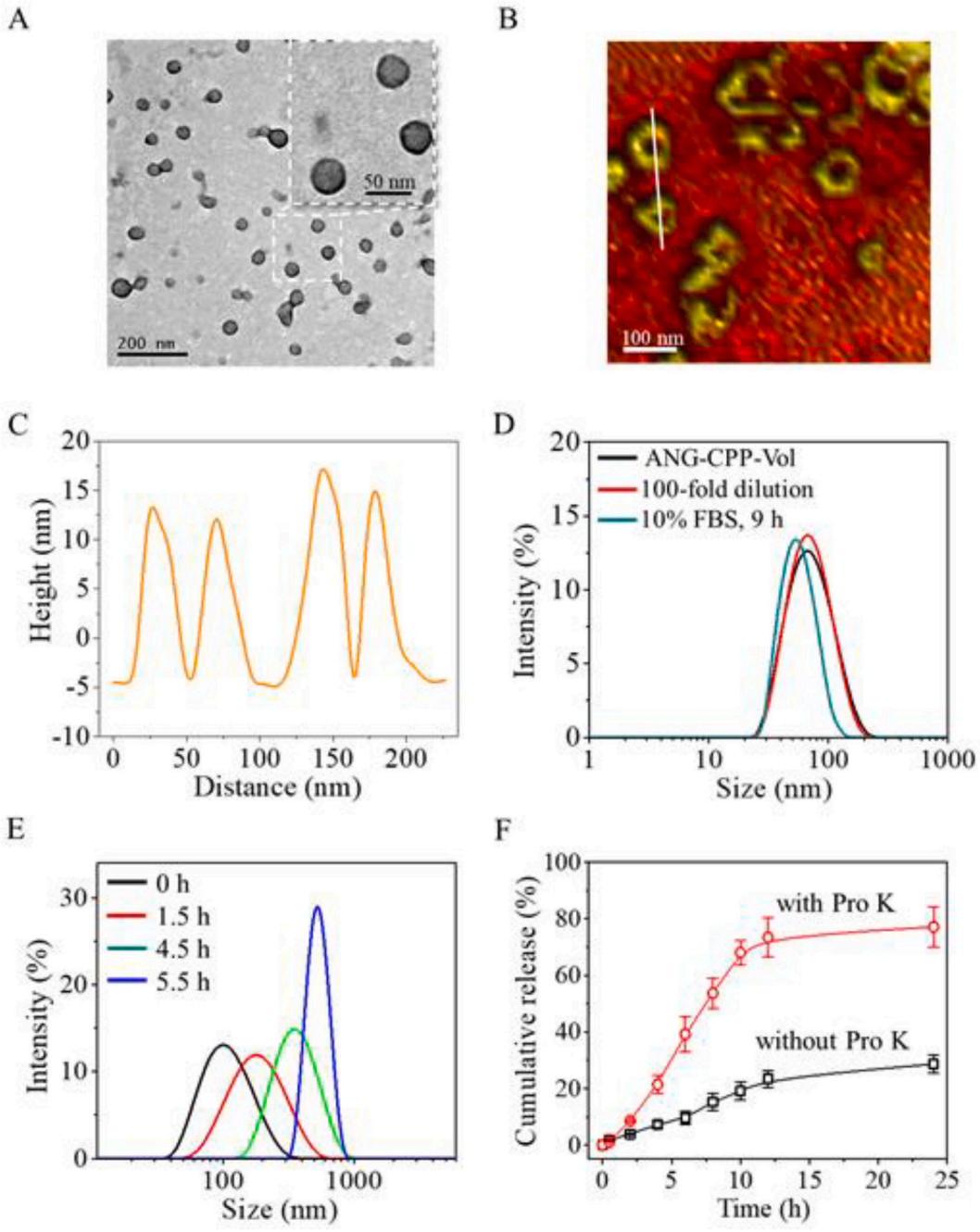

Fig. 2. Characterization of blank ANG-CPP and ANG-CPP-Vol with 13.9 wt% of Vol. (A-C) Morphology of ANG-CPP measured by TEM (A) and AFM (B). (C) Cross-sectional height profile along the line in (B). (D) Size distribution and stability of ANG-CPP-Vol against 10% FBS, dilution, and long-term storage at a concentration of 1.0 mg/mL. (E) Size changes of ANG-CPP-Vol in PB with 6.0 units/mL of proteinase K. (F) *In vitro* Vol release profile from ANG-CPP-Vol and CPP-Vol in the presence of proteinase K (6.0 units/mL).

Table 2
Characterization of ANG-CPP-Vol.

Entry	DLC (wt%)		DLE[a] (%)	Size[b] (nm)	PDI[b]	ξ[c] (mV)
	Theo.	Determ.[a]				
1	5.0	3.5	70.5	63	0.12	−13.5
2	10.0	7.3	72.5	71	0.12	−9.6
3	20.0	13.9	69.3	76	0.15	−7.9

[a] Determined by UV–vis measurement.
[b] Determined by DLS (1.0 mg/mL, 25 °C).
[c] Determined by electrophoresis in PB (1.0 mg/mL, 25 °C).

Following the addition of different Vol formulations in the upper chamber, the U-87 MG cells in the lower chamber were collected within 24 h and analyzed by flow cytometry. Fig. 3E demonstrates 4.0-fold higher cellular uptake of ANG-CPP-Vol than CPP-Vol, signifying that ANG functionalization facilitates the BBB transcytosis and cellular uptake of CPP-Vol in U-87 MG cells.

3.4. Cytotoxicity and cell cycle arrest of ANG-CPP-Vol

MTT assay revealed that free Vol, CPP-Vol, and ANG-CPP-Vol had obvious cytotoxicity against U-87 MG cells, among which ANG-CPP-Vol displayed a half-maximal inhibitory concentration (IC_{50}) of 0.19 μg/mL,

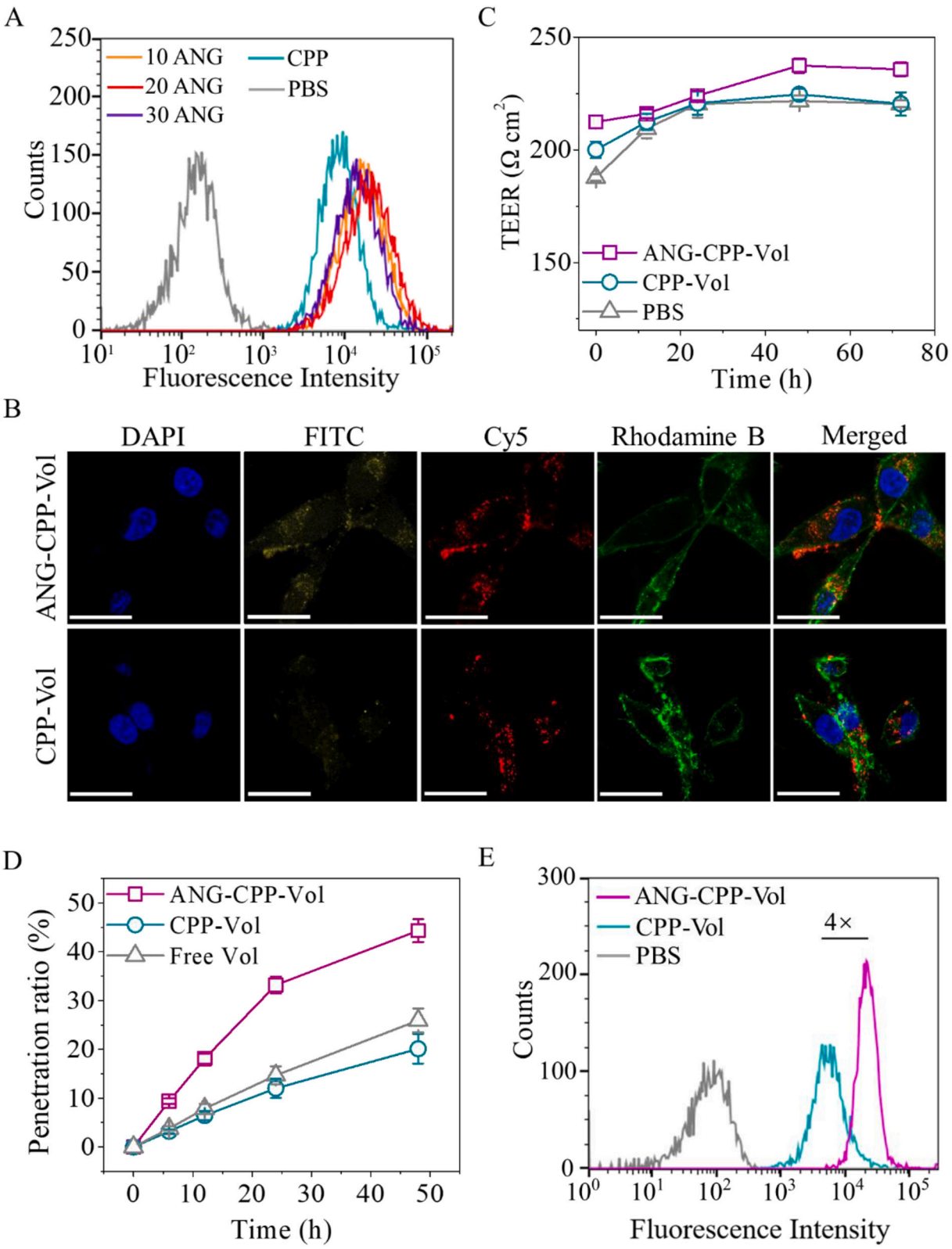

Fig. 3. (A) Flow cytometry measurement of U-87 MG cells following 4 h incubation with Cy5-labled CPP-Vol and ANG-CPP-Vol. (B) Confocal images of U-87 MG cells following 4 h incubation with Cy5-labled CPP-Vol/FITC and ANG-CPP-Vol/FITC. Scale bar: 25 nm. (C) TEER of bEnd.3 cells monolayer monitored using an epithelial voltmeter ($n = 3$). (D) *In vitro* BBB transcytosis behaviors of different formulations with time measured by fluorescence spectrometer. (E) Cellular uptake behaviors of CPP-Vol and ANG-CPP-Vol in U-87 MG cells within 24 h following penetration of the *in vitro* BBB model.

which was 3.4-fold lower than CPP-Vol (0.64 μg/mL) and 7.8-fold lower than free Vol (1.49 μg/mL) (Fig. 4A). The superior inhibition activity of ANG-CPP-Vol toward U-87 MG cells is related to its enhanced cellular uptake (Fig. 3A and Fig. S6). Colony formation assay demonstrated that the proliferation of U-87 MG cells was inhibited by ANG-CPP-Vol within 14 d (Fig. S8). Interestingly, ANG-CPP-Vol exhibited little cytotoxicity toward normal cells like L929 fibroblasts even at a high Vol concentration of 20 μg/mL (Fig. S9A), mainly because normal cells usually display low expression of both Plk1 and LRP-1 receptor. Previous report shows that Vol has potent inhibition on Plk1 with an IC_{50} of 0.87 nmol/L (0.54 μg/mL), while possesses little effect on other protein kinases even at a high concentration of 10 μmol/L (6.2 mg/mL) [36], affording superior selectivity and less systemic toxicity in comparison with chemotherapeutic agents. Of note, blank ANG-CPP and CPP induced no obvious inhibition of U-87 MG cells (Fig. S9B), signifying that ANG-CPP is non-toxic. Many previous studies have demonstrated that poly(L-tyrosine) and poly(L-aspartic acid)-based vehicles possess excellent biocompatibility [57–62].

Vol has been reported to interfere with the progression of mitosis including centrosome maturation, spindle formation, and chromosome segregation by inhibiting Plk1, inducing G2/M phase arrest in cancer cells [36]. Fig. 4B reveals that free Vol, CPP-Vol, and ANG-CPP-Vol at a Vol concentration of 0.25 μg/mL all induced significant G2/M phase arrest of U-87 MG cells. Remarkably, complete G2/M phase arrest in cancer cells was attained by ANG-CPP-Vol, mainly owing to enhanced endocytosis. Considering that cancer cells with G2/M phase arrest are much more sensitive to radiation [63–65], ANG-CPP-Vol might be employed not only as a novel nanodrug, but also as a radiosensitizer for cancer radiotherapy. Western blot analysis confirmed that free Vol, CPP-Vol, and ANG-CPP-Vol could downregulate the level of Plk1 in U-87 MG cells (Fig. 4C), in which ANG-CPP-Vol revealed the strongest Plk1 downregulation effect that was elevated as the concentrations of Vol increased from 0.05 to 0.5 μg/mL. Benefiting from the enhanced cellular uptake conferred by ANG-docked nanovehicles and selective inhibition of Plk1 in U87 cancer cells by Vol, ANG-CPP-Vol provides an innovative and safe therapeutic strategy for GBM.

3.5. *In vivo* pharmacokinetics and biodistribution

As shown in Fig. 5A, CPP-Vol and ANG-CPP-Vol prominently extended the elimination half-life of free Vol from 0.38 h to 3.3 h and 3.5 h, respectively (Fig. 5A), supporting that ANG-CPP-Vol is stable in circulation. Owing to short half-lives, molecular targeted drugs are often administered at high dose and frequency for a long period [32,66]. For biodistribution study, orthotopic GBM model was established by inoculating cut U-87 MG-Luc tumor tissue into the left striatum of mice and monitored by tracking Luc bioluminescence. Following 10-day inoculation, clear bioluminescence was visualized in the brain (Fig. 5B), verifying the successful establishment of orthotopic GBM. *In vivo* near-infrared fluorescence imaging showed that mice treated with Cy5-ANG-CPP-Vol displayed strong Cy5 fluorescence at tumor sites following 4 h administration, and the fluorescence density increased with time and reached the highest at 12 h (Fig. 5B), suggesting that significant amount of Cy5-ANG-CPP-Vol could cross BBB and reside in U-87 MG-Luc tumors. In contrast, little Cy5 fluorescence was observed in the brain of mice treated with CPP-Vol, signifying the critical role of ANG on brain delivery. It should be mentioned that Cy5 signal in brain decayed following 24 h treatment with Cy5-ANG-CPP-Vol, which might

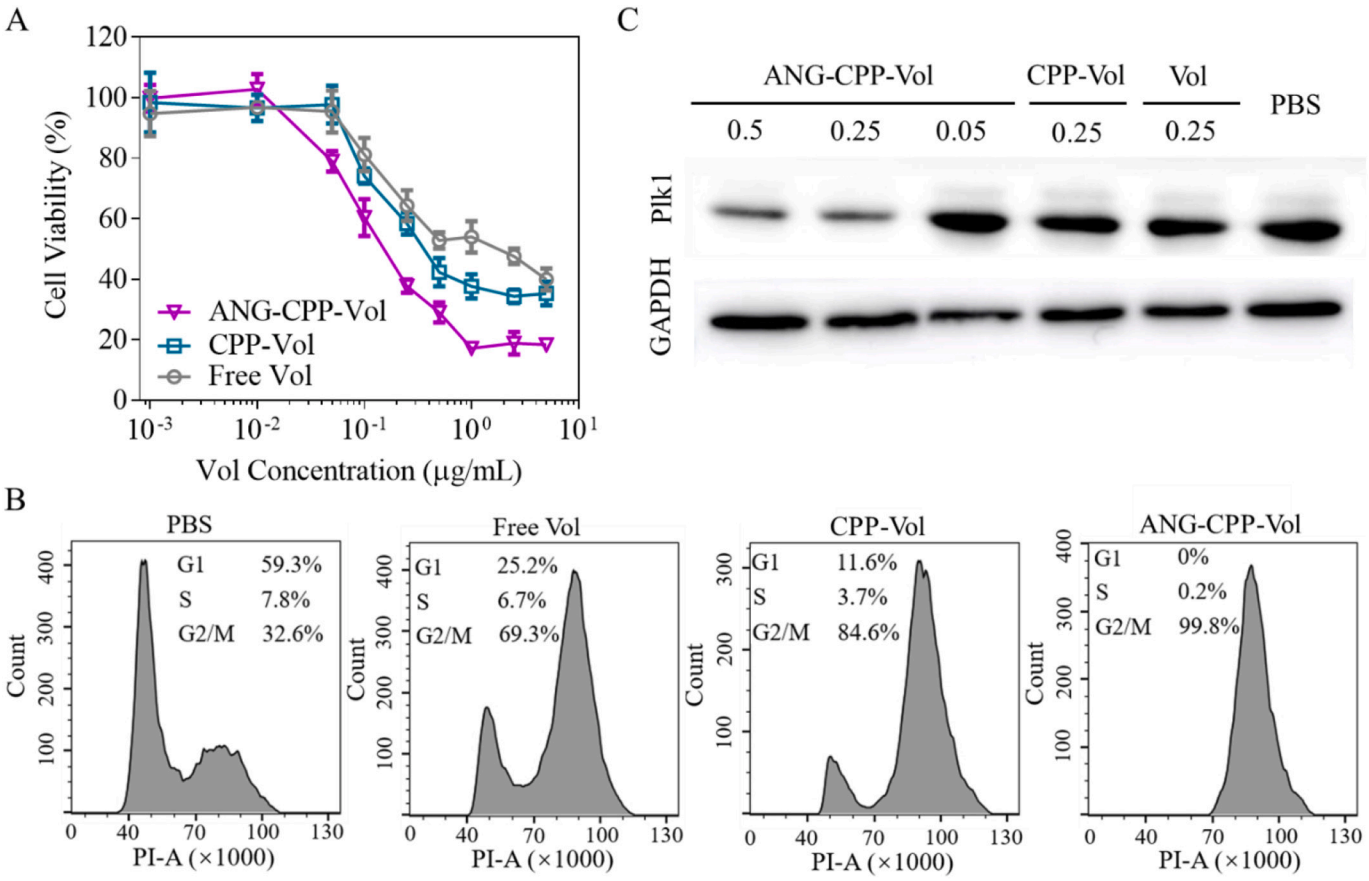

Fig. 4. Antiproliferative activity of ANG-CPP-Vol in U-87 MG cells. (A) MTT assay. U-87 MG cells were incubated with ANG-CPP-Vol for 4 + 68 h. (B) Cell cycle arrest. Cells were incubated with different formulations (Vol concentration: 0.25 μg/mL) for 4 + 44 h; (C) Western blot analysis. Cells were treated with PBS, free Vol (0.25 μg/mL), CPP-Vol (0.25 μg/mL), and ANG-CPP-Vol (0.5, 0.25, 0.05 μg/mL) for 4 + 20 h.

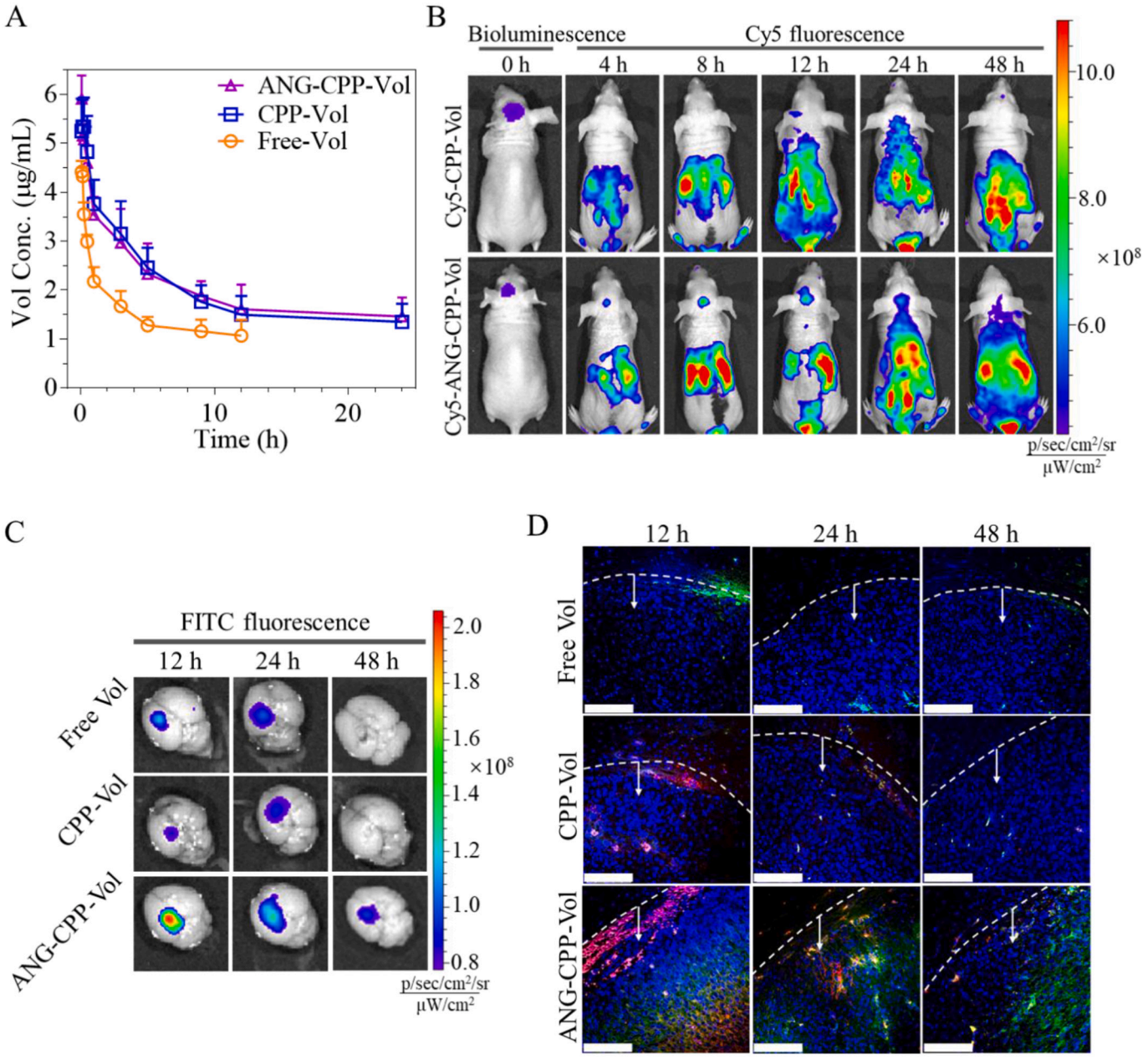

Fig. 5. (A) *In vivo* pharmacokinetics of free Vol/FITC, CPP-Vol/FITC, and ANG-CPP-Vol/FITC in BALB/c mice following i.v. injection. (B) Bioluminescence of orthotopic U-87 MG-Luc GBM xenografts and *in vivo* fluorescence imaging of tumor-bearing mice treated with different Cy5-labeled formulations. (C) *Ex vivo* fluorescence imaging of orthotopic GBM xenografts. (D) Immunohistochemical fluorescence images of GBM sections taken from mice treated with different formulations. GBM area in section images was marked by white arrows (under the white dash line). Vol was labeled with FITC (green) and nanovehicles were labeled with Cy5 (red). Scale bar: 100 μm. (For interpretation of the references to colour in this figure legend, the reader is referred to the web version of this article.)

be attributed to the enzymatic degradation of PTyr and PAsp polypeptides under tumor environments, generating Cy5-containing small fragments that could leak out of the brain with time. *Ex vivo* imaging further confirmed that mice treated with Cy5-ANG-CPP-Vol/FITC had far higher drug accumulation at the GBM sites within 12–48 h than free Vol/FITC and Cy5-CPP-Vol/FITC (Fig. 5C). Immunohistochemical fluorescence images showed that ANG-CPP-Vol distributed deep into the tumor following 12 h administration (Fig. 5D). More importantly, the separation of green fluorescence (FITC-labeled Vol) from red fluorescence (Cy5-labeled ANG-CPP) indicated fast release of Vol from ANG-CPP-Vol. Nearly complete drug release was seen at 48 h (Fig. S10). In contrast, both CPP-Vol and free Vol displayed scarce distribution into the tumor, confirming that ANG-CPP plays an important role in delivering Vol to GMB.

3.6. *In vivo* therapeutic efficacy

The *in vivo* therapeutic efficacy of ANG-CPP-Vol was explored in orthotopic U-87 MG-Luc tumor-bearing nude mice. In sharp contrast to fast increase of tumor bioluminescence in PBS group, mice treated with free Vol, CPP-Vol, and ANG-CPP-Vol all displayed weakened bioluminescence within 8 days (Fig. 6A), signifying all Vol formulations could to some extent suppress the tumor growth. On day 12, remarkable tumor bioluminescence was observed in both free Vol and CPP-Vol groups, while ANG-CPP-Vol group displayed negligible elevation of bioluminescence, corroborating that with the help of ANG targeting ligand, molecular targeted agent (Vol) can efficiently penetrate BBB, actively reach GBM tumor tissue, and significantly suppress the tumor growth. The semi-quantitative analysis revealed that mice treated with ANG-

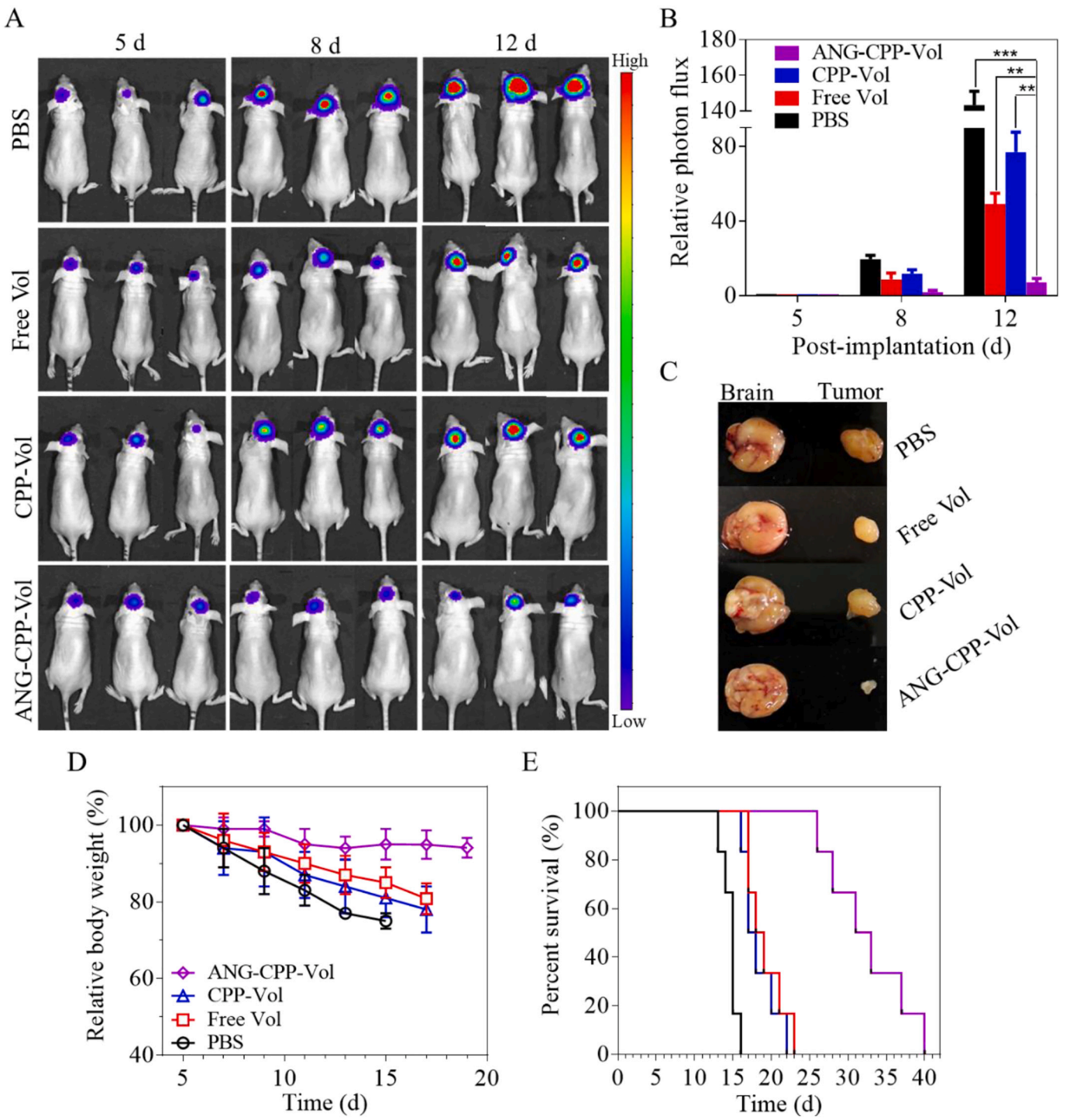

Fig. 6. *In vivo* antitumor efficacy of ANG-CPP-Vol toward orthotopic U-87 MG-Luc GBM-bearing nude mice ($n = 6$). Mice were administered at 10 mg Vol equiv./kg *via* tail vein injection every 2 days for 6 times. (A) Bioluminescence images in mice treated with different formulations at a dose of 10 mg Vol equiv./kg. (B) Mean U-87 MG-Luc luminescence levels of orthotopic U-87 MG-Luc GBM (**$p < 0.01$, ***$p < 0.001$, one-way ANOVA). (C) Images of brains and tumors harvested from orthotopic GBM-bearing nude mice on day 14. (D) Relative body weight changes. (E) Kaplan-Meier survival curves of mice. ANG-CPP-Vol *v.s.* PBS, Free Vol, or CPP-Vol, ***$p < 0.001$ (Kaplan-Meier analysis, log-rank test).

CPP-Vol had eleven- and seven-times lower tumor bioluminescence on day 12 in comparison with those treated with CPP-Vol and free Vol, respectively (Fig. 6B). The superb therapeutic efficacy of ANG-CPP-Vol was further verified by its smallest tumor blocks and relatively intact brain structure of mice on day 14, as shown in Fig. 6C. In comparison, mice treated with free Vol, CPP-Vol and PBS presented much larger tumor blocks and deformed brain tissue due to the invasion of malignant GBM. The development of GBM in free Vol, CPP-Vol and PBS groups was further verified by continuous decrease of body weight of mice (Fig. 6D). In contrast, mice treated with ANG-CPP-Vol exhibited little body weight loss during the whole experimental period. Kaplan-Meier survival analysis displayed that free Vol and CPP-Vol slightly improved the survival time of GBM-bearing mice (Fig. 6E). Of note, mice treated with ANG-CPP-Vol displayed significant survival advantages with an

extended median survival time of 31 days, which was over two times longer than PBS group. These initial treatment results are very encouraging because most anti-GBM therapies were reported to give only moderate survival benefits [52,67–69]. H&E staining clearly showed that ANG-CPP-Vol caused negligible damage to main organs including heart, liver, spleen, kidney, and lung (Fig. S11), signifying that nanodrugs formed from molecular targeted agents have remarkable *in vivo* safety. Given its low toxicity, we could further increase the dose and/or number of injections, which might greatly boost the anti-GBM effects of ANG-CPP-Vol. Moreover, ANG-CPP-Vol would also be interesting to combine with radiation therapy and to combat drug resistance [34,70].

4. Conclusions

The present study has demonstrated that angiopep-2-docked polypeptide-based chimaeric polymersome (ANG-CPP) can efficiently load, transport and release Plk1 inhibitor, volasertib (Vol), into orthotopic U-87 MG GBM xenografts in mice, leading to highly efficacious tumor repression, substantial survival advantages, and negligible toxic effects. ANG-CPP-Vol offers a novel and highly appealing molecular therapy for GBM in that (i) a majority of GBM cells overexpress Plk1 and suppression of Plk1 would cause potent anti-GBM effects; (ii) Vol, as a targeted molecular drug and with low off-target toxicity, is clinically used for treating AML patients; (iii) ANG-CPP-Vol is featured with small size, high stability, pronounced BBB permeability, GBM-selectivity, and speedy cytoplasmic Vol release; and importantly (iv) ANG-CPP-Vol can be easily fabricated. This brain delivery of Vol has emerged as a promising treatment modality for GBM.

Credit author statement

Z.Y. Zhong and C. Deng: Conceptualization, Funding acquisition, Project administration, Resources, Supervision, Validation, Writing – review & editing. Q.Y. Fan: Data curation, Formal analysis, Investigation, Methodology, Writing – original draft. Y.Y. Liu and G.H. Cui: Methodology. All authors discussed the results and commented on the manuscript.

Acknowledgments

The financial support from the National Natural Science Foundation of China (NSFC 51973149, 51773145, and 51761135117) and the Natural Science Foundation of the Jiangsu Higher Education Institutions of China (19KJA220002) is acknowledged.

Appendix A. Supplementary data

Supplementary data to this article can be found online at https://doi.org/10.1016/j.jconrel.2020.10.043.

References

[1] R.L. Siegel, K.D. Miller, A. Jemal, Cancer statistics, 2020, CA Cancer J. Clin. 70 (2020) 7–30.
[2] M.L. Broekman, S.L.N. Maas, E.R. Abels, T.R. Mempel, A.M. Krichevsky, X. O. Breakefield, Multidimensional communication in the microenvirons of glioblastoma, Nat. Rev. Neurol. 14 (2018) 482–495.
[3] A. Shergalis, A. Bankhead, U. Luesakul, N. Muangsin, N. Neamati, Current challenges and opportunities in treating glioblastoma, Pharmacol. Rev. 70 (2018) 412–445.
[4] S. Valdebenito, D. D'Amico, E. Eugenin, Novel approaches for glioblastoma treatment: focus on tumor heterogeneity, treatment resistance, and computational tools, Cancer Rep. 2 (2019), e1220.
[5] B.K. Ahir, H.H. Engelhard, S.S. Lakka, Tumor development and angiogenesis in adult brain tumor: Glioblastoma, Mol. Neurobiol. 57 (2020) 2461–2478.
[6] L. Jena, E. McErlean, H. McCarthy, Delivery across the blood-brain barrier: Nanomedicine for glioblastoma multiforme, Drug Deliv. Transl. Res. 10 (2020) 304–318.
[7] D. Furtado, M. Björnmalm, S. Ayton, A.I. Bush, K. Kempe, F. Caruso, Overcoming the blood–brain barrier: the role of nanomaterials in treating neurological diseases, Adv. Mater. 30 (2018), 1801362.
[8] M. Luo, G. Lewik, J.C. Ratcliffe, C.H.J. Choi, E. Mäkilä, W.Y. Tong, N.H. Voelcker, Systematic evaluation of transferrin-modified porous silicon nanoparticles for targeted delivery of doxorubicin to glioblastoma, ACS Appl. Mater. Interfaces 11 (2019) 33637–33649.
[9] P. Bourassa, W. Alata, C. Tremblay, S. Paris-Robidas, F. Calon, Transferrin receptor-mediated uptake at the blood–brain barrier is not impaired by Alzheimer's disease neuropathology, Mol. Pharm. 16 (2019) 583–594.
[10] Y. Wei, X. Gu, Y. Sun, F. Meng, G. Storm, Z. Zhong, Transferrin-Binding Peptide Functionalized Polymersomes Mediate Targeted Doxorubicin Delivery to Colorectal Cancer in vivo 319, 2020, pp. 407–415.
[11] S. Quader, X. Liu, Y. Chen, P. Mi, T. Chida, T. Ishii, Y. Miura, N. Nishiyama, H. Cabral, K. Kataoka, cRGD peptide-installed epirubicin-loaded polymeric micelles for effective targeted therapy against brain tumors, J. Control. Release 258 (2017) 56–66.
[12] Y. Zhu, J. Zhang, F. Meng, C. Deng, R. Cheng, J. Feijen, Z. Zhong, cRGD-functionalized reduction-sensitive shell-sheddable biodegradable micelles mediate enhanced doxorubicin delivery to human glioma xenografts in vivo, J. Control. Release 233 (2016) 29–38.
[13] W. Chen, Y. Zou, Z. Zhong, R. Haag, Cyclo(RGD)-decorated reduction-responsive nanogels mediate targeted chemotherapy of integrin overexpressing human glioblastoma in vivo, Small 13 (2017) 1601997.
[14] M. Qiu, H. Sun, F. Meng, R. Cheng, J. Zhang, C. Deng, Z. Zhong, Lipopepsomes: a novel and robust family of nano-vesicles capable of highly efficient encapsulation and tumor-targeted delivery of doxorubicin hydrochloride in vivo, J. Control. Release 272 (2018) 107–113.
[15] X. Cai, A. Bandla, C.K. Chuan, G. Magarajah, L.-D. Liao, D.B.L. Teh, B.K. Kennedy, N.V. Thakor, B. Liu, Identifying glioblastoma margins using dual-targeted organic nanoparticles for efficient in vivo fluorescence image-guided photothermal therapy, Mater. Horiz. 6 (2019) 311–317.
[16] H.S. Min, H. Kim, M. Naito, S. Ogura, K. Toh, K. Hayashi, B. Kim, S. Fukushima, Y. Anraku, K. Miyata, K. Kataoka, Systemic brain delivery of antisense oligonucleotides across the blood-brain barrier with a glucose-installed polymeric nanocarrier, Angew. Chem. Int. Ed. 59 (2020) 8173–8180.
[17] Y. Anraku, H. Kuwahara, Y. Fukusato, A. Mizoguchi, T. Ishii, K. Nitta, Y. Matsumoto, K. Toh, K. Miyata, S. Uchida, K. Nishina, K. Osada, K. Itaka, N. Nishiyama, H. Mizusawa, T. Yamasoba, T. Yokota, K. Kataoka, Glycaemic control boosts glucosylated nanocarrier crossing the BBB into the brain, Nat. Commun. 8 (2017) 1001.
[18] A.R. Neves, J.F. Queiroz, S.A.C. Lima, S. Reis, Apo E-functionalization of solid lipid nanoparticles enhances brain drug delivery: uptake mechanism and transport pathways, Bioconjug. Chem. 28 (2017) 995–1004.
[19] Y. Jiang, J. Zhang, F. Meng, Z. Zhong, Apolipoprotein E peptide-directed chimeric polymersomes mediate an ultrahigh-efficiency targeted protein therapy for glioblastoma, ACS Nano 12 (2018) 11070–11079.
[20] H. Qin, Y. Jiang, J. Zhang, C. Deng, Z. Zhong, Oncoprotein inhibitor rigosertib loaded in apoe-targeted smart polymersomes reveals high safety and potency against human glioblastoma in mice, Mol. Pharm. 16 (2019) 3711–3719.
[21] C.-F. Cho, J.M. Wolfe, C.M. Fadzen, D. Calligaris, K. Hornburg, E.A. Chiocca, N.Y. R. Agar, B.L. Pentelute, S.E. Lawler, Blood-brain-barrier spheroids as an in vitro screening platform for brain-penetrating agents, Nat. Commun. 8 (2017) 15623.
[22] A. Joseph, C. Contini, D. Cecchin, S. Nyberg, L. Ruiz-Perez, J. Gaitzsch, G. Fullstone, X. Tian, J. Azizi, J. Preston, G. Volpe, G. Battaglia, Chemotactic synthetic vesicles: design and applications in blood-brain barrier crossing, Sci. Adv. 3 (2017), e1700362.
[23] J.S. Kim, D.H. Shin, J.-S. Kim, Dual-targeting immunoliposomes using angiopep-2 and CD133 antibody for glioblastoma stem cells, J. Control. Release 269 (2018) 245–257.
[24] L.L. Israel, O. Braubach, A. Galstyan, A. Chiechi, E.S. Shatalova, Z. Grodzinski, H. Ding, K.L. Black, J.Y. Ljubimova, E. Holler, A combination of tri-leucine and angiopep-2 drives a polyanionic polymalic acid nanodrug platform across the blood–brain barrier, ACS Nano 13 (2019) 1253–1271.
[25] X. Dong, Current strategies for brain drug delivery, Theranostics 8 (2018) 1481–1493.
[26] Y. Zou, Y. Liu, Z. Yang, D. Zhang, Y. Lu, M. Zheng, X. Xue, J. Geng, R. Chung, B. Shi, Effective and targeted human orthotopic glioblastoma xenograft therapy via a multifunctional biomimetic nanomedicine, Adv. Mater. 30 (2018), 1803717.
[27] H. Gao, S. Zhang, S. Cao, Z. Yang, Z. Pang, X. Jiang, Angiopep-2 and activatable cell-penetrating peptide dual-functionalized nanoparticles for systemic glioma-targeting delivery, Mol. Pharm. 11 (2014) 2755–2763.
[28] Y. Zhu, Y. Jiang, F. Meng, C. Deng, R. Cheng, J. Zhang, J. Feijen, Z. Zhong, Highly efficacious and specific anti-glioma chemotherapy by tandem nanomicelles co-functionalized with brain tumor-targeting and cell-penetrating peptides, J. Control. Release 278 (2018) 1–8.
[29] J. Tao, W. Fei, H. Tang, C. Li, C. Mu, H. Zheng, F. Li, Z. Zhu, Angiopep-2-conjugated "core–shell" hybrid nanovehicles for targeted and ph-triggered delivery of arsenic trioxide into glioma, Mol. Pharm. 16 (2019) 786–797.
[30] E.L. Rhun, M. Preusser, P. Roth, D.A. Reardon, M.J.V. Den Bent, P.Y. Wen, G. Reifenberger, M.J.C.T.R. Weller, Molecular targeted therapy of glioblastoma, Cancer Treat. Rev. 80 (2019), 101896.
[31] Y.T. Lee, Y.J. Tan, C.E. Oon, Molecular targeted therapy: treating cancer with specificity, Eur. J. Pharmacol. 834 (2018) 188–196.
[32] C.Y. Lee, Strategies of temozolomide in future glioblastoma treatment, Onco Targets Ther. 10 (2017) 265–270.

[33] E.G. Graham-Gurysh, A.B. Murthy, K.M. Moore, S.D. Hingtgen, E.M. Bachelder, K. M. Ainslie, Synergistic Drug Combinations for a Precision Medicine Approach to Interstitial Glioblastoma Therapy 323, 2020, pp. 282–292.
[34] M. Rabé, S. Dumont, A. Álvarez-Arenas, H. Janati, J. Belmonte-Beitia, G.F. Calvo, C. Thibault-Carpentier, Q. Séry, C. Chauvin, N. Joalland, F. Briand, S. Blandin, E. Scotet, C. Pecqueur, J. Clairambault, L. Oliver, V. Perez-Garcia, A. Nadaradjane, P.-F. Cartron, C. Gratas, F.M. Vallette, Identification of a transient state during the acquisition of temozolomide resistance in glioblastoma, Cell Death Dis. 11 (2020) 19.
[35] F. Higuchi, A.L. Fink, J. Kiyokawa, J.J. Miller, M.V.A. Koerner, D.P. Cahill, H. Wakimoto, PLK1 inhibition targets Myc-activated malignant glioma cells irrespective of mismatch repair deficiency–mediated acquired resistance to temozolomide, Mol. Cancer Ther. 17 (2018) 2551–2563.
[36] J. Van den Bossche, F. Lardon, V. Deschoolmeester, I. De Pauw, J.B. Vermorken, P. Specenier, P. Pauwels, M. Peeters, A. Wouters, Spotlight on volasertib: Preclinical and clinical evaluation of a promising Plk1 inhibitor, Med. Res. Rev. 36 (2016) 749–786.
[37] D. Hiraoka, E. Hosoda, K. Chiba, T. Kishimoto, SGK phosphorylates Cdc25 and Myt1 to trigger cyclin B-Cdk1 activation at the meiotic G2/M transition, J. Cell Biol. 218 (2019) 3597–3611.
[38] Y. Matthess, M. Raab, R. Knecht, S. Becker, K. Strebhardt, Sequential Cdk1 and Plk1 phosphorylation of caspase-8 triggers apoptotic cell death during mitosis, Mol. Oncol. 8 (2014) 596–608.
[39] C. Moison, V.P. Lavallée, C. Thiollier, B. Lehnertz, I. Boivin, N. Mayotte, Y. Gareau, M. Fréchette, V. Blouin-Chagnon, S. Corneau, S. Lavallée, S. Lemieux, A. Marinier, J. Hébert, G. Sauvageau, Complex karyotype AML displays G2/M signature and hypersensitivity to PLK1 inhibition, Blood Adv. 3 (2019) 552–563.
[40] J. Van den Bossche, A. Domen, M. Peeters, C. Deben, I. De Pauw, J. Jacobs, S. De Bruycker, P. Specenier, P. Pauwels, J.B. Vermorken, F. Lardon, A. Wouters, Radiosensitization of non-small cell lung cancer cells by the Plk1 inhibitor volasertib is dependent on the p53 status, Cancers 11 (2019) 1893.
[41] X. Xin, F. Lin, Q. Wang, L. Yin, R.I. Mahato, ROS-responsive polymeric micelles for triggered simultaneous delivery of PLK1 inhibitor/miR-34a and effective synergistic therapy in pancreatic cancer, ACS Appl. Mater. Interfaces 11 (2019) 14647–14659.
[42] X. Gu, Y. Wei, Q. Fan, H. Sun, R. Cheng, Z. Zhong, C. Deng, cRGD-decorated biodegradable polytyrosine nanoparticles for robust encapsulation and targeted delivery of doxorubicin to colorectal cancer in vivo, J. Control. Release 301 (2019) 110–118.
[43] S. Xue, X. Gu, J. Zhang, H. Sun, C. Deng, Z. Zhong, Construction of small-sized, robust, and reduction-responsive polypeptide micelles for high loading and targeted delivery of chemotherapeutics, Biomacromolecules 19 (2018) 3586–3593.
[44] Y. Shi, D.M. Roy, B. Theek, E. Oude Blenke, E.H.E. Pieters, M.H.A.M. Fens, J. Ehling, R.M. Schiffelers, G. Storm, C.F. Van Nostrum, Complete regression of xenograft tumors upon targeted delivery of paclitaxel via Π–Π stacking stabilized polymeric micelles, ACS Nano 9 (2015) 3740–3752.
[45] Y. Wang, Y. Wu, K. Li, S. Shen, Z. Liu, D. Wu, Ultralong circulating lollipop-like nanopartides assembled with cossypol, doxorubicin, and polydopamine via π-π stacking for synergistic tumor therapy, Adv. Funct. Mater. 29 (2019) 1805582.
[46] X. Gu, M. Qiu, H. Sun, J. Zhang, L. Cheng, C. Deng, Z. Zhong, Polytyrosine nanoparticles enable ultra-high loading of doxorubicin and rapid enzyme-responsive drug release, Biomater. Sci. 6 (2018) 1526.
[47] X. Wu, Y. Wu, H. Ye, S. Yu, C. He, X. Chen, Interleukin-15 and cisplatin co-encapsulated thermosensitive polypeptide hydrogels for combined immuno-chemotherapy, J. Control. Release 255 (2017) 81–93.
[48] Y. Ren, H. Luo, H. Huang, N. Hakulinen, T. Tu, Improving the catalytic performance of proteinase K from Parengyodontium album for use in feather degradation, Int. J. Biol. Macromol. 154 (2020) 1586–1595.
[49] L. Maletinska, E.A. Blakely, K.A. Bjornstad, D.F. Deen, L. Knoff, T.M. Forte, Human glioblastoma cell lines: levels of low-density lipoprotein receptor and low-density lipoprotein receptor-related protein, Cancer Res. 60 (2000) 2300–2303.
[50] S. Gao, H. Tian, Z. Xing, D. Zhang, Y. Guo, Z. Guo, X. Zhu, X. Chen, A non-viral suicide gene delivery system traversing the blood brain barrier for non-invasive glioma targeting treatment, J. Control. Release 243 (2016) 357–369.
[51] A.R. Khan, X. Yang, M. Fu, G. Zhai, Recent progress of drug nanoformulations targeting to brain, J. Control. Release 291 (2018) 37–64.
[52] Y. Jiang, W. Yang, J. Zhang, F. Meng, Z. Zhong, Protein toxin chaperoned by LRP-1-targeted virus-mimicking vesicles induces high-efficiency glioblastoma therapy in vivo, Adv. Mater. 30 (2018), 1800316.
[53] Y. Shi, Y. Jiang, J. Cao, W. Yang, J. Zhang, F. Meng, Z. Zhong, Boosting RNAi therapy for orthotopic glioblastoma with nontoxic brain-targeting chimaeric polymersomes, J. Control. Release 292 (2018) 163–171.
[54] H. Ruan, Z. Chai, Q. Shen, X. Chen, B. Su, C. Xie, C. Zhan, S. Yao, H. Wang, M. Zhang, M. Ying, W. Lu, A novel peptide ligand RAP12 of LRP1 for glioma targeted drug delivery, J. Control. Release 279 (2018) 306–315.
[55] Q. Lu, X. Cai, X. Zhang, S. Li, Y. Song, D. Du, P. Dutta, Y. Lin, Synthetic polymer nanoparticles functionalized with different ligands for receptor-mediated transcytosis across the blood–brain barrier, ACS Appl. Bio Mater. 1 (2018) 1687–1694.
[56] T. Tian, J. Li, C. Xie, Y. Sun, H. Lei, X. Liu, J. Xia, J. Shi, L. Wang, W. Lu, C. Fan, Targeted imaging of brain tumors with a framework nucleic acid probe, ACS Appl. Mater. Interfaces 10 (2018) 3414–3420.
[57] H. Cabral, K. Miyata, K. Osada, K. Kataoka, Block copolymer micelles in nanomedicine applications, Chem. Rev. 118 (2018) 6844–6892.
[58] Z. Song, Z. Han, S. Lv, C. Chen, L. Chen, L. Yin, J. Cheng, Synthetic polypeptides: from polymer design to supramolecular assembly and biomedical application, Chem. Soc. Rev. 46 (2017) 6570–6599.
[59] T. Deming, Synthesis of side-chain modified polypeptides, Chem. Rev. 116 (2016) 786–808.
[60] C. He, X. Zhuang, Z. Tang, H. Tian, X. Chen, Stimuli-sensitive synthetic polypeptide-based materials for drug and gene delivery, Adv. Healthc. Mater. 1 (2012) 48–78.
[61] C. Deng, J. Wu, R. Cheng, F. Meng, H. Klok, Z. Zhong, Functional polypeptide and hybrid materials: precision synthesis via α-amino acid N-carboxyanhydride polymerization and emerging biomedical applications, Prog. Polym. Sci. 39 (2014) 330–364.
[62] H. Sun, X. Gu, Q. Zhang, H. Xu, Z. Zhong, C. Deng, Cancer nanomedicines based on synthetic polypeptides, Biomacromolecules 20 (2019) 4299–4311.
[63] Q. Ran, Y. Xiang, P. Stephen, C. Wu, T. Li, S.-X. Lin, Z. Li, CRIF1–CDK2 interface inhibitors: an unprecedented strategy for modulation of cell radiosensitivity, J. Am. Chem. Soc. 141 (2019) 1420–1424.
[64] X. Cheng, X. Zhang, P. Liu, L.-Y. Xia, Y.-W. Jiang, G. Gao, H.-Y. Wang, Y.-H. Li, N. Ma, H.-H. Ran, F.-G. Wu, Sequential treatment of cell cycle regulator and nanoradiosensitizer achieves enhanced radiotherapeutic outcome, ACS Appl. Bio Mater. 2 (2019) 2050–2059.
[65] S. Gao, W. Zhang, R. Wang, S.P. Hopkins, J.C. Spagnoli, M. Racin, L. Bai, L. Li, W. Jiang, X. Yang, C. Lee, K. Nagata, E.W. Howerth, H. Handa, J. Xie, Q. Ma, A. Kumar, Nanoparticles encapsulating nitrosylated maytansine to enhance radiation therapy, ACS Nano 14 (2020) 1468–1481.
[66] F. Doz, F. Locatelli, A. Baruchel, N. Blin, B. De Moerloose, D. Frappaz, M. Dworzak, M. Fischer, J. Stary, R. Fuertig, K. Riemann, T. Taube, D. Reinhardt, I. Phase, Dose-escalation study of volasertib in pediatric patients with acute leukemia or advanced solid tumors, Pediatr, Blood Cancer 66 (2019) e27900.
[67] L.P. Ganipineni, F. Danhier, V. Préat, Drug delivery challenges and future of chemotherapeutic nanomedicine for glioblastoma treatment, J. Control. Release 281 (2018) 42–57.
[68] D. Ran, J. Mao, C. Zhan, C. Xie, H. Ruan, M. Ying, J. Zhou, W.-L. Lu, W. Lu, D-Retroenantiomer of quorum-sensing peptide-modified polymeric micelles for brain tumor-targeted drug delivery, ACS Appl. Mater. Interfaces 9 (2017) 25672–25682.
[69] P. Kadiyala, D. Li, F.M. Nuñez, D. Altshuler, R. Doherty, R. Kuai, M. Yu, N. Kamran, M. Edwards, J.J. Moon, P.R. Lowenstein, M.G. Castro, A. Schwendeman, High-density lipoprotein-mimicking nanodiscs for chemo-immunotherapy against glioblastoma multiforme, ACS Nano 13 (2019) 1365–1384.
[70] C.-P. Wu, C.-H. Hsieh, S.-H. Hsiao, S.-Y. Luo, C.-Y. Su, Y.-Q. Li, Y.-H. Huang, C.-W. Huang, S.-C. Hsu, Human ATP-binding cassette transporter ABCB1 confers resistance to volasertib (BI 6727), a selective inhibitor of polo-like kinase 1, Mol. Pharm. 12 (2015) 3885–3895.